

ScRNA-seq and bulk RNA-seq reveal the characteristics of ferroptosis and establish a risk signature in cholangiocarcinoma

Wenchao Yao,^{1,2,3} Xuxu Liu,^{1,2,3} Yuanhang He,^{1,2} Maolan Tian,^{1,2} Shixin Lu,^{1,2} Qiang Wang,^{1,2} Yi Zheng,^{1,2} Zhenyi Lv,^{1,2} Chenjun Hao,^{1,2} Dongbo Xue,^{1,2} and Xianzhi Meng^{1,2}

¹Department of General Surgery, the First Affiliated Hospital of Harbin Medical University, Harbin, China; ²Key Laboratory of Hepatosplenic Surgery, Ministry of Education, the First Affiliated Hospital of Harbin Medical University, Harbin, China

Ferroptosis is a recently discovered mode of cell death that inhibits tumor growth. Single-cell RNA sequencing (scRNA-seq) is a powerful tool for analyzing tumor heterogeneity and the immune microenvironment at the single-cell level. We used CIBERSORT to identify cellular immune scores and found that monocytes had significantly infiltrated and were correlated with prognosis in cholangiocarcinoma. scRNA-seq data were extracted from the Gene Expression Omnibus database, and the FindCluster() package was used for cell cluster analysis, which obtained 21 cell clusters, and there was increased TNFSF13B-TFRC intercellular communication between monocytes and cholangiocytes. A weighted correlation network analysis was performed with the WGCNA package to obtain monocyte-related gene modules. Univariate and multivariate Cox analyses were then performed to further establish the signature, and the reliability of the signature was assessed by receiver operating characteristic curve and decision curve analysis. A nomogram signature based on the Kaplan-Meier survival analysis was established. We found that the communication between monocytes and malignant cells in cholangiocarcinoma may be a regulatory factor of ferroptosis in cancer cells. The prognostic stratification system of the three-gene signature related to monocytes and ferroptosis can accurately assess the prognostic risk for cholangiocarcinoma.

INTRODUCTION

Cholangiocarcinoma (CHOL) is a highly malignant invasive carcinoma originating from cholangiocytes, and its incidence is currently increasing worldwide.¹ CHOL has an insidious onset, is highly invasive, and can invade perihepatic tissues and lymph nodes and create distant metastases.² Most patients with CHOL are at an advanced stage when they are first diagnosed, and despite the availability of various treatment options, the overall prognosis for patients remains poor.³ Although a variety of genetic prognostic signatures have been used to assess tumor risk, there is still a lack of accurate and reliable prognostic biomarkers for CHOL to guide treatment and provide personalized management, which is one of the reasons why the prognosis of CHOL has not improved.⁴ Therefore, early molecular diagnosis and prognosis of CHOL are of great significance for improving the survival of patients.

Ferroptosis is a type of programmed cell death caused by Fe-dependent lipid peroxidation and plays an important role in inhibiting tumor cell proliferation, invasion, and metastasis.⁵ Ferroptosis can trigger an immune response in tumors, particularly in malignancies that are resistant to conventional treatments.⁶ Ferroptosis has a dual role in cancer because ferroptotic tumor cells release signaling molecules that can promote or inhibit tumor proliferation.⁷ At present, ferroptosis has been widely studied in various cancers such as gastric, lung, pancreatic, and ovarian cancers and glioblastoma.^{8–12} However, the role of these ferroptosis molecules in CHOL is not fully understood. Therefore, it is necessary to explore the application value of ferroptosis to CHOL.

In recent years, with the rapid development of single-cell sequencing technology, researchers have studied the biochemical processes and pathogenesis of some diseases at the single-cell level.¹³ Single-cell sequencing technology has been widely used in tumor, inflammation, and other disease processes as well as stem cell development, differentiation, and other physiological processes.¹⁴ Single-cell sequencing can study tumors from various perspectives such as tumor heterogeneity, the tumor microenvironment, tracking the metastasis and spread of cancer cells, and understanding the evolution of cancer cell resistance during drug treatment.^{15,16} Min Zhang et al. demonstrated the heterogeneity of CHOL and the unique tumor microenvironment through single-cell RNA sequencing (scRNA-seq) technology and expounded on the heterogeneity of various types of immune cells, stromal cells, and malignant cells in the tumor microenvironment, which is the main cause of CHOL. The immune microenvironment provides a detailed landscape.¹⁷ In addition, scRNA-seq can also enable researchers to penetrate the tumor microenvironment based on cell-specific changes in the transcriptome and further

Received 13 June 2022; accepted 22 September 2022;
<https://doi.org/10.1016/j.omto.2022.09.008>.

³These authors contributed equally

Correspondence: Xianzhi Meng, Department of General Surgery, the First Affiliated Hospital of Harbin Medical University, Harbin, China.

E-mail: mengxianzhi@hrbmu.edu.cn

Correspondence: Dongbo Xue, Department of General Surgery, the First Affiliated Hospital of Harbin Medical University, Harbin, China.

E-mail: xuedongbo@hrbmu.edu.cn

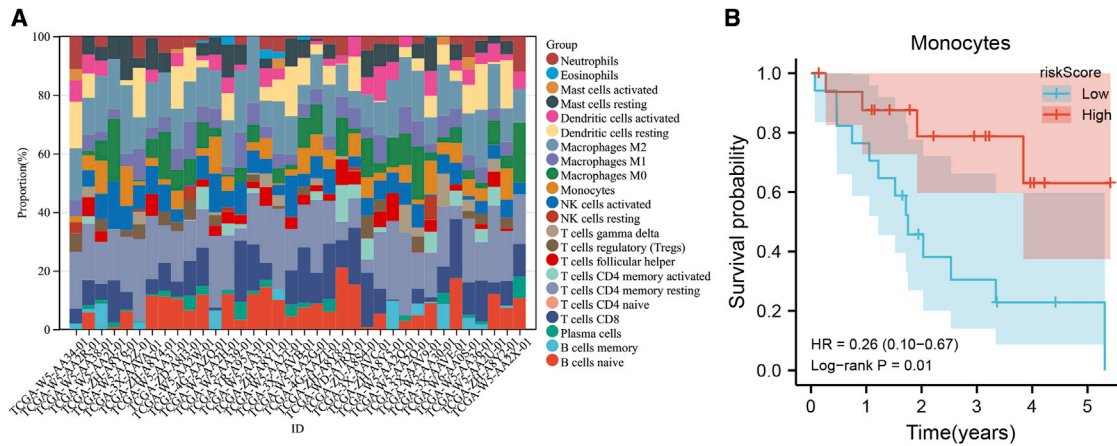


Figure 1. The proportion of immune cells

(A) The proportion of 22 immune cells built on RNA-seq data. (B) The Kaplan-Meier curves (overall survival) of patients with different proportions of monocytes.

develop diagnostic and prognostic markers to aid in the precise diagnosis and treatment of patients.¹⁸ However, the application of single-cell sequencing data in the diagnosis and prognosis of CHOL is still limited, particularly in combination with the bulk data and corresponding prognostic information in public databases.

In this study, we fully explored the role of ferroptosis in CHOL and its association with the tumor microenvironment by exploring scRNA-seq data in the Gene Expression Omnibus (GEO) database and by combining the bulk data in The Cancer Genome Atlas (TCGA) and GEO with the clinical information of CHOL patients. Finally, we established the importance of ferroptosis-related genes and monocytes in the tumor microenvironment in the prognosis of CHOL. A prognostic signature based on ferroptosis and monocytes was established, which can accurately assess the prognosis of patients with CHOL, thereby allowing personalized management for patients with CHOL.

RESULTS

CIBERSORT analysis

To evaluate the role of various immune cell infiltrates in CHOL, we analyzed the proportion of immune cells and their impact on the prognosis of CHOL using bulk RNA-seq data. CIBERSORT is an analytical tool that predicts the proportion of 22 immune cells based on RNA-seq data from the TCGA database (Figure 1A). In addition, a survival analysis showed that patients with and without a high abundance of monocyte cells had a better prognosis ($p = 0.01$) (Figure 1B). In response to this phenomenon, we conducted an in-depth analysis of the infiltration of monocytes in CHOL.

scRNA-seq analysis suggests communication between monocytes and CHOL cells

The scRNA-seq dataset (GEO: GSE138709) was used to delineate the diversity and heterogeneity of various cell subsets in CHOL tissue. Nonlinear dimensionality reduction was performed using Uniform Manifold Approximation and Projection, and cells were clustered us-

ing the FindCluster() function, resulting in 22 clusters (Figure 2A). Cholangiocytes (clusters 0, 2, and 5; markers STMN1, KRT19, and CLDN4) and monocytes (cluster 3; markers S100A9, S100A8, and LYZ) were classified according to cell markers (Figure 2B).

To investigate the effect of monocyte infiltration on CHOL cells, we performed an intercellular communication analysis between monocytes and cholangiocytes in CHOL samples. The heatmap of all intercellular communication showed that the communication between cholangiocytes and endothelial cells was the most prominent, which is also consistent with the function of liver sinusoidal endothelial cells under normal physiological conditions. The second most prominent communication was between cholangiocytes and monocytes, macrophages (Figure 2C). By analyzing the communication relationship between monocytes and cholangiocytes in detail, it was found that the relationship between TNFSF13B and TFRC was significant (Figure 2D, $p < 0.01$, mean = 0.293). The number of occurrences of this relationship pair ranks 21st among all the intercellular relationship pairs, which is sufficient to show its high frequency (Figure 2E). Jiao Wu et al. reported in *Nature* that intercellular interactions can activate NF2-YAP-TFRC signaling to regulate ferroptosis in cancer cells.¹⁹ We speculate that monocytes can initiate the ferroptosis pathway in CHOL cells through intercellular communication. Therefore, we performed a KEGG (Kyoto Encyclopedia of Genes and Genomes) functional enrichment analysis on the marker genes of this cell subset, but the significantly enriched pathways did not include the ferroptosis pathway (Figure 2F).

scRNA-seq analysis of subdivided subpopulations within CHOL cells

Because we did not find a TFRC-related ferroptosis signaling pathway in the functional enrichment of CHOL cells, we continued to subdivide the cell subsets of CHOL cells and obtained a total of nine clusters (Figure 3A). The marker genes of each cell subset are shown in Figure 3B. According to the heatmap analysis of ferroptosis gene signatures retrieved from the KEGG database, the enrichment of

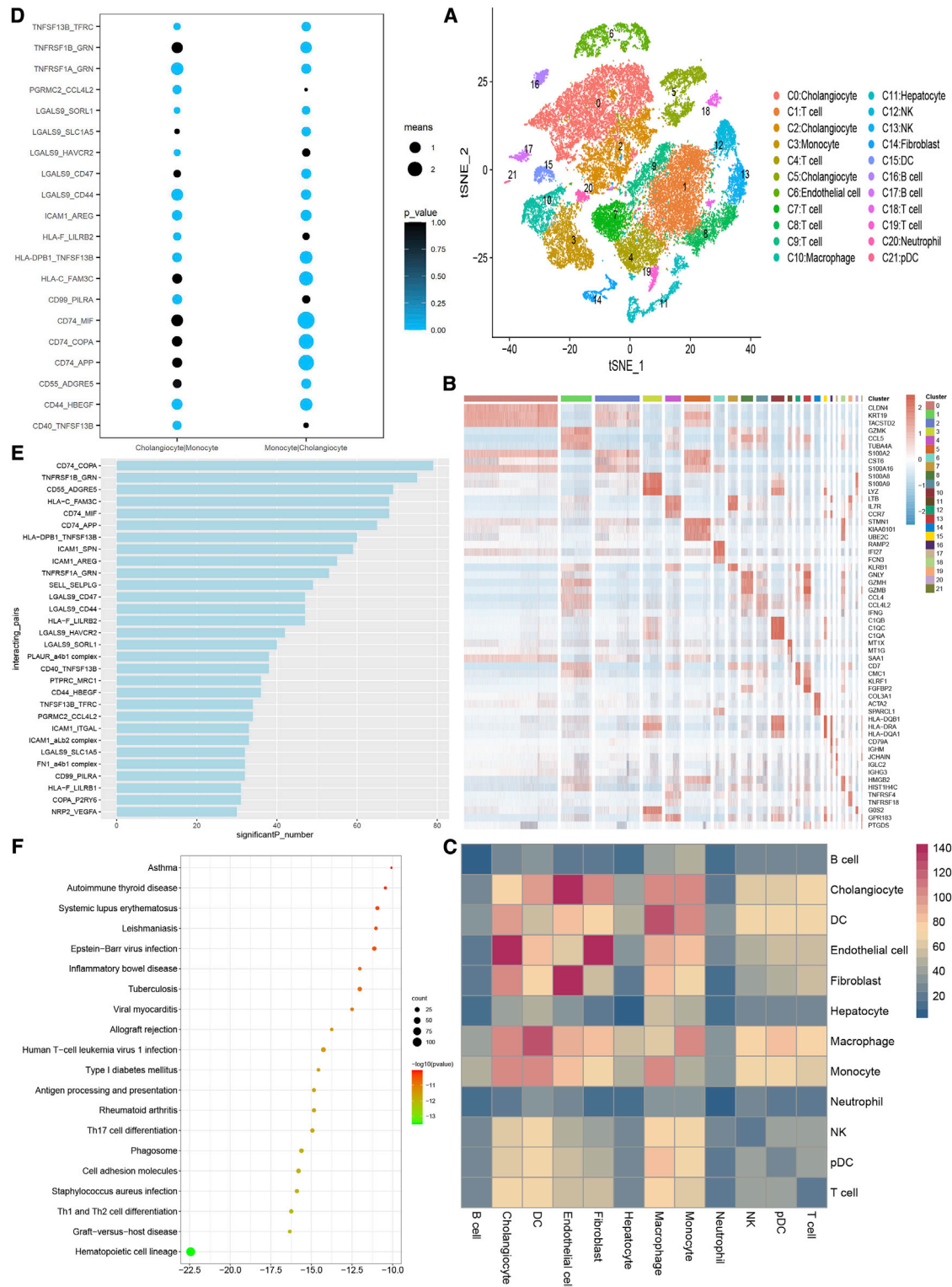


Figure 2. Dissection of CHOL with scRNA-seq

(A) tSNE plot of 40,919 cells from five tumor tissues and three adjacent tissues (label colors are according to separate clusters and cells.) (B) Marker genes heatmap of each cell subpopulation. (C) Heatmap of all cellular communications. (D) Point plot of interacting pairs between monocytes and cholangiocytes. (E) The top 30 interacting pairs of all cells. (F) KEGG functional enrichment analysis of marker genes in CHOL cells.

ferroptosis genes in C0, C1, C3, C4, C5, C7, and C8 was higher, and the TFRC gene was significantly overexpressed in the C4 subgroup. The enrichment of ferroptosis genes was significantly lower in C2 and C6, and the TFRC gene was significantly underexpressed in the C6 subpopulation (Figure 3C). Correspondingly, a contrast number variation (CNV) analysis showed that C0, C1, C3, C4, C5, C7, and C8 had higher degrees of copy number mutations, suggesting that they were malignant cell subsets. C2 and C6 had lower degrees of copy number mutations, suggesting that they are benign subpopulations of cells (Figure 3D).

We performed a KEGG functional enrichment analysis on the marker genes of the C4 and C6 subgroups. The significantly enriched pathways in C4 were mainly proteoglycans in cancer, pathways in cancer, transcriptional misregulation in cancer, and a variety of metabolism-related pathways (Figure 3E); the significantly enriched pathways in C6 were mainly tryptophan metabolism, fatty acid degradation, glycolysis/gluconeogenesis, and other metabolic pathways (Figure 3F). Most of the pathways in C4 are directly related to cancer, whereas those in C6 are not directly related to cancer, which again confirms the results of benign and malignant identification of cell subsets inferred from CNV. Based on the significantly high expression of TFRC in C4 and its significantly low expression in C6, we screened all genes that were significantly upregulated in C4 and significantly downregulated in C6 for functional enrichment analysis (Figure 3G). The results showed that phagosome, the IL-17 signaling pathway, the TNF signaling pathway, necroptosis, and other pathways were enriched, and the enrichment degree of ferroptosis ranked in the top five.

These results showed that compared with that in benign cells, the ferroptosis pathway was significantly enriched in CHOL cells; monocytes initiated ferroptosis in some of the cancer cell clusters through communication with CHOL cells (TNFSF13B-TFRC).

WGCNA of gene sets associated with monocyte infiltration

To further explore the potential role of monocytes in CHOL, we performed weighted gene co-expression analysis (WGCNA) on CHOL-based TCGA data, constructed a co-expression network, and identified co-expression modules (Figures 4A and 4B). Based on two evaluation perspectives, scale independence and mean connectivity, we identified the appropriate soft threshold ability from the scale-free topological model fit (R^2) to classify the monocyte infiltration-related gene set into 29 modules (Figure 4C). The dark turquoise and tan modules (552 genes in total) were significantly associated with monocyte infiltration ($p < 0.05$), and the results showed a negative correlation with high monocyte infiltration and a positive correlation with low infiltration.

We also obtained 388 ferroptosis-related genes from the FerrDb database. These two modular gene sets intersected with the differentially expressed gene sets and were then merged (Figure 4D), and a total of 473 gene sets related to ferroptosis or monocyte infiltration were obtained (Figure 4E).

Construction of prognostic risk signature

First, by performing a univariate Cox analysis on these 473 genes, the monocyte and ferroptosis-related gene signature was screened ($p < 0.05$ was the threshold), and there were nine genes in total (Figure 5A). A multivariate Cox regression analysis was then performed on the nine genes associated with the prognosis, and a three-gene prognosis signature was constructed (Figure 5B).

The model formula is as follows:

$$\text{Risk Score} = \sum_{i=1}^n C_i \times \text{Exp}_i,$$

where $n = 3$, Exp_i is the expression of the three genes, and C_i is the corresponding coefficient. $\text{RiskScore} = 1.543 \times \text{Expression (BNIP3)} + 1.758 \times \text{Expression (TMEM107)} + 1.576 \times \text{Expression (CENPW)}$. The coefficients of BNIP3, TMEM107, and CENPW were obtained by multivariate Cox regression, which were BNIP3 (1.543), TMEM107 (1.758), and CENPW (1.576) respectively.

The protein-protein interaction network map was constructed for these three genes and their related genes, and the genes with higher correlations were mainly BNIP3L, RHEB, and CENP family genes and TMEM family genes (Figure 5C).

Based on the expression values and correlation coefficients of these three genes, a prognostic risk score was calculated for each patient sample. Figures 5D and 5E show the total risk score (upper figure), survival time (middle figure), and single-gene expression levels (lower figure) for the TCGA-CHOL and GEO: GSE107943 datasets. Based on the risk score for each patient shown in Figures 5D and 5E, the patients were divided into high- and low-risk groups using the optimal cut off value.

Predictive performance validation on training and validation datasets

To verify the prognostic performance of the ferroptosis-monocyte (F-M) signature on different data platforms, TCGA-CHOL was used as the training set, and GSE107943 was used as the validation set. Figures 6A and 6C are the Kaplan-Meier (K-M) survival curves of TCGA-CHOL and GSE107943, respectively. The survival outcomes of patients with CHOL were significantly different in both datasets (log rank $p < 0.01$). The receiver operating characteristic (ROC) curve was used to evaluate the sensitivity and specificity of the F-M signature for patient prognosis. The results showed that the TCGA-CHOL dataset performed better, with areas under the curve (AUCs) of 0.866, 0.869, and 0.933 for 1, 3, and 5 years, respectively (Figure 6B). The AUCs of the GSE107943 dataset for 1 year, 3 years, and 5 years were 0.618, 0.792, and 0.910, respectively (Figure 6D). We also re-evaluated the performance of this prognostic signature in predicting 1-, 3-, and 5-year survival using decision curve analysis (DCA) based on the clinical data attached to the TCGA data. The results showed that the F-M signature had better predictive power than other clinical information at 1, 3, and 5 years (Figures 6E–6G).

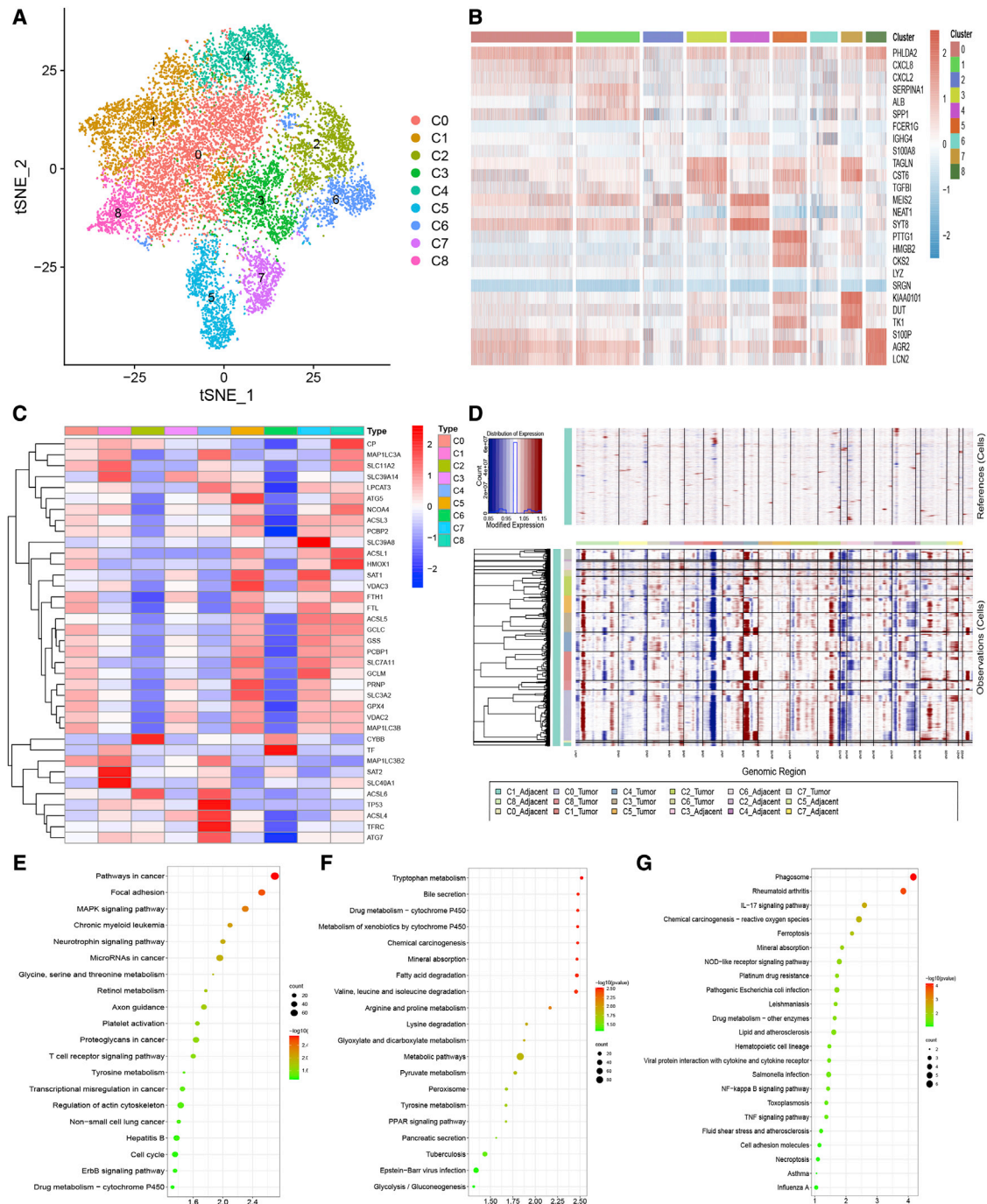


Figure 3. Characteristic analysis of cholangiocytes with scRNA-seq

(A) tSNE plot of all cholangiocytes. (B) Marker genes heatmap of each cholangiocytes' subset. (C) Heatmap of ferroptosis signature expression in each cholangiocytes' subset. (D) Large-scale CNVs of single cells (rows) of cholangiocytes. CNVs were inferred from transcriptomes. Red, amplifications; blue, deletions. (E–F) KEGG functional enrichment analysis of marker genes in cluster 4 (E) and cluster 6 (F). (G) KEGG functional enrichment analysis of genes that upregulated in cluster 4 and downregulated in cluster 6.

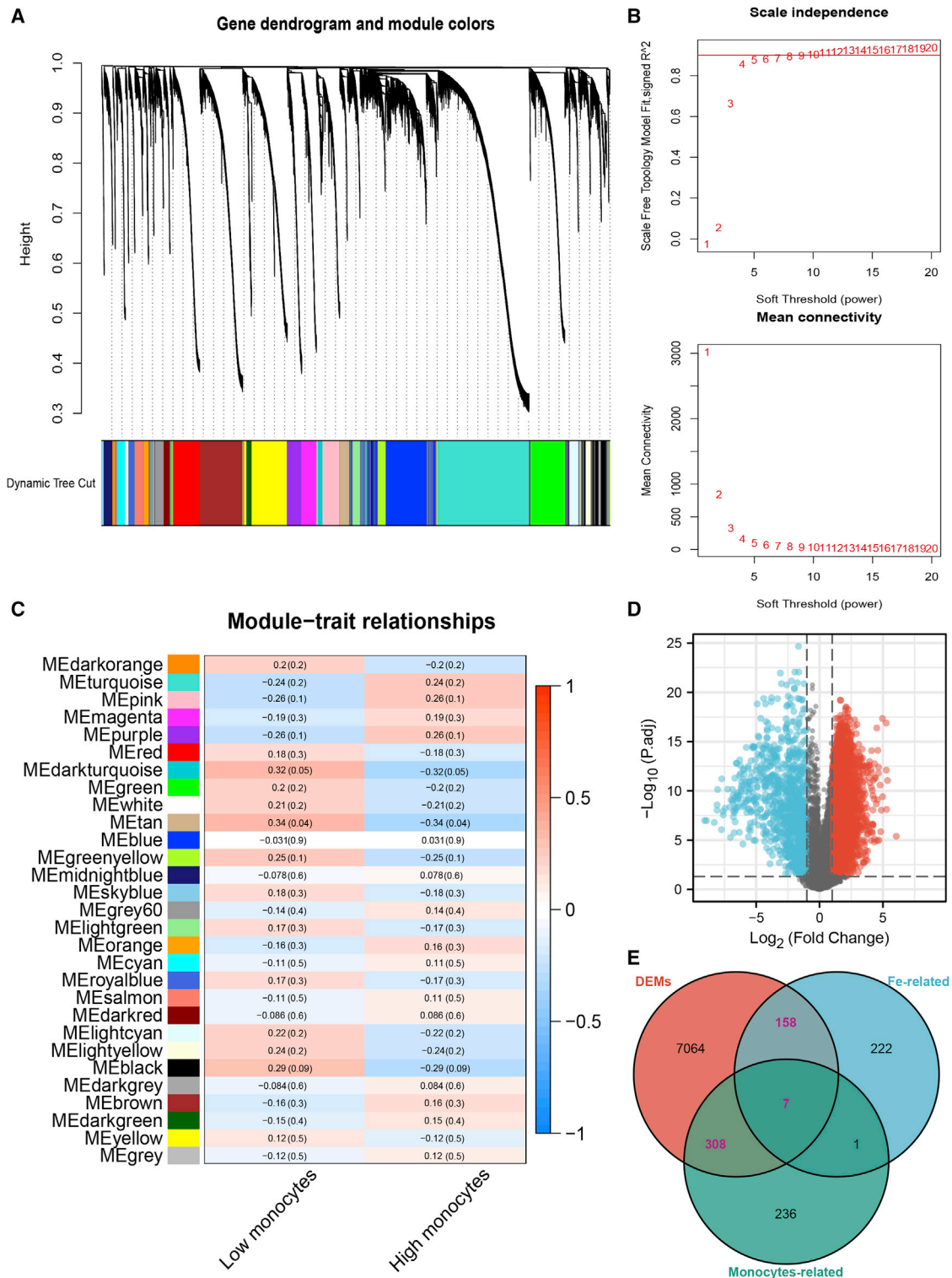


Figure 4. Screening of monocyte-related genes

(A) Genes are clustered into discrete modules. (B) The nature of the network topology constructed with unique power values. (C) The correlation between different modules and the proportion of monocyte-high and low infiltration. (D) Volcano plot of differentially expressed genes (DEGs) in TCGA-CHOL. (E) Venn plot of DEGs, ferroptosis-related genes, and monocyte-related genes.

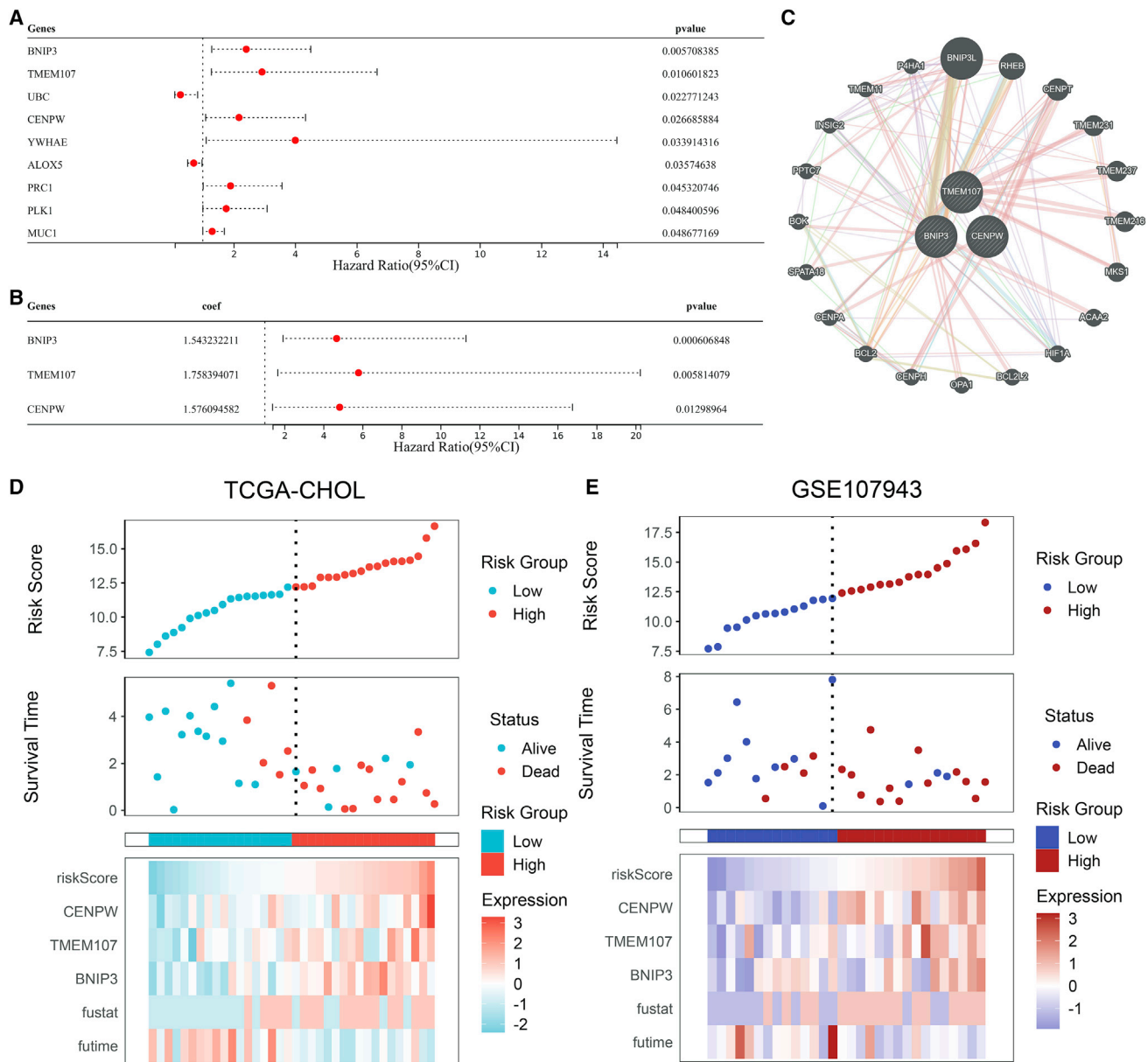


Figure 5. Construct a risk model

(A) Nine prognostic genes were screened from the 473 genes by univariate Cox analysis. (B) Three prognostic genes were screened from the nine genes by multivariate Cox analysis. (C) Protein-protein interaction network of the three genes. (D, E) Distributions of risk scores and survival status of CHOL patients in the training and test datasets.

Construction of the nomogram signature based on K-M survival analysis and GSEA

To realize the application potential of the signature, we integrated the risk score into the nomogram (Figure 7A). The nomogram calibration curve showed that the actual observed values were in good agreement with the predicted values (Figure 7B). In fact, the nomogram risk assessment map can also combine the risk score with the clinical characteristics to achieve better clinical application value. In addition, we

performed a survival analysis based on the K-M score for single genes. Figures 7C–7E shows the survival analysis based on the expression levels of BNIP3, TMEM107, and CENPW. The low expression group of the three genes had a better prognosis, among which BNIP3 and TMEM107 had significant prognostic results, whereas CENPW had a $p = 0.074$. These results suggest that BNIP3 and TMEM107 also have a certain ability as single genes to differentiate the survival time of patients, whereas CENPW cannot.

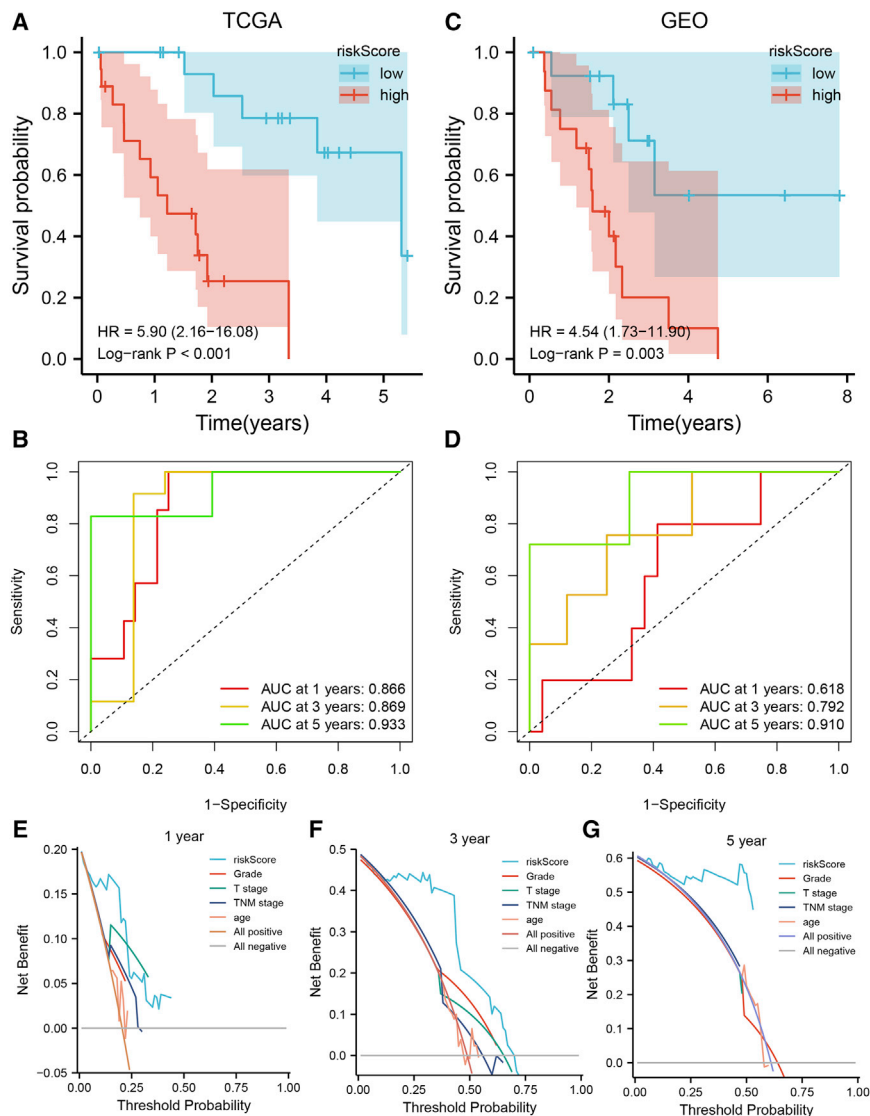


Figure 6. Validation of predictive performance of training and test datasets

(A, C) Survival curve of high- and low-risk group in training and test datasets. (B, D) ROC curves of signature for predicting 1-, 3-, and 5-year survival in training and test datasets. (E–G) DCA curves of signature (compared with clinical information) for predicting 1-, 3-, and 5-year survival in train dataset.

attention given to the interaction between cancer cells that undergo ferroptosis and the immune microenvironment. It has been reported that ferroptotic tumor cells promote the recruitment of anticancer immune cells such as CD8+ T cells and natural killer (NK) cells by releasing danger signals and downregulating the infiltration level of tumor-promoting cells (such as myeloid-derived suppressor cells). In addition, CD8+ T cells and NK cells induce cancer cell ferroptosis by secreting GzmA and GzmB, and CD8+ T cells induce tumor cell ferroptosis by secreting interferon- γ .²³ Continued accumulation of monocyte-derived macrophages leads to overexpression of ALOX5 and accumulation of the metabolite LTB₄, which triggers the expression of the ferroptosis-promoting gene ACSL4 in lung epithelial cells.²⁴ These studies suggest that, as an important subset of immune cells, monocytes may also participate in the ferroptosis of malignant cells through intercellular communication.

In recent years, research on ferroptosis in CHOL has gradually increased. Jin-Yi et al. reported that glutathione peroxidase-regulated ferroptosis through cysteine modification depletes reduced glutathione in bile as a possible mechanism for extrahepatic CHOL.²⁵ There are also several articles on prognostic gene signatures of ferroptosis in CHOL, but these articles do not delve into the possible mechanisms of ferroptosis in CHOL.^{26–28}

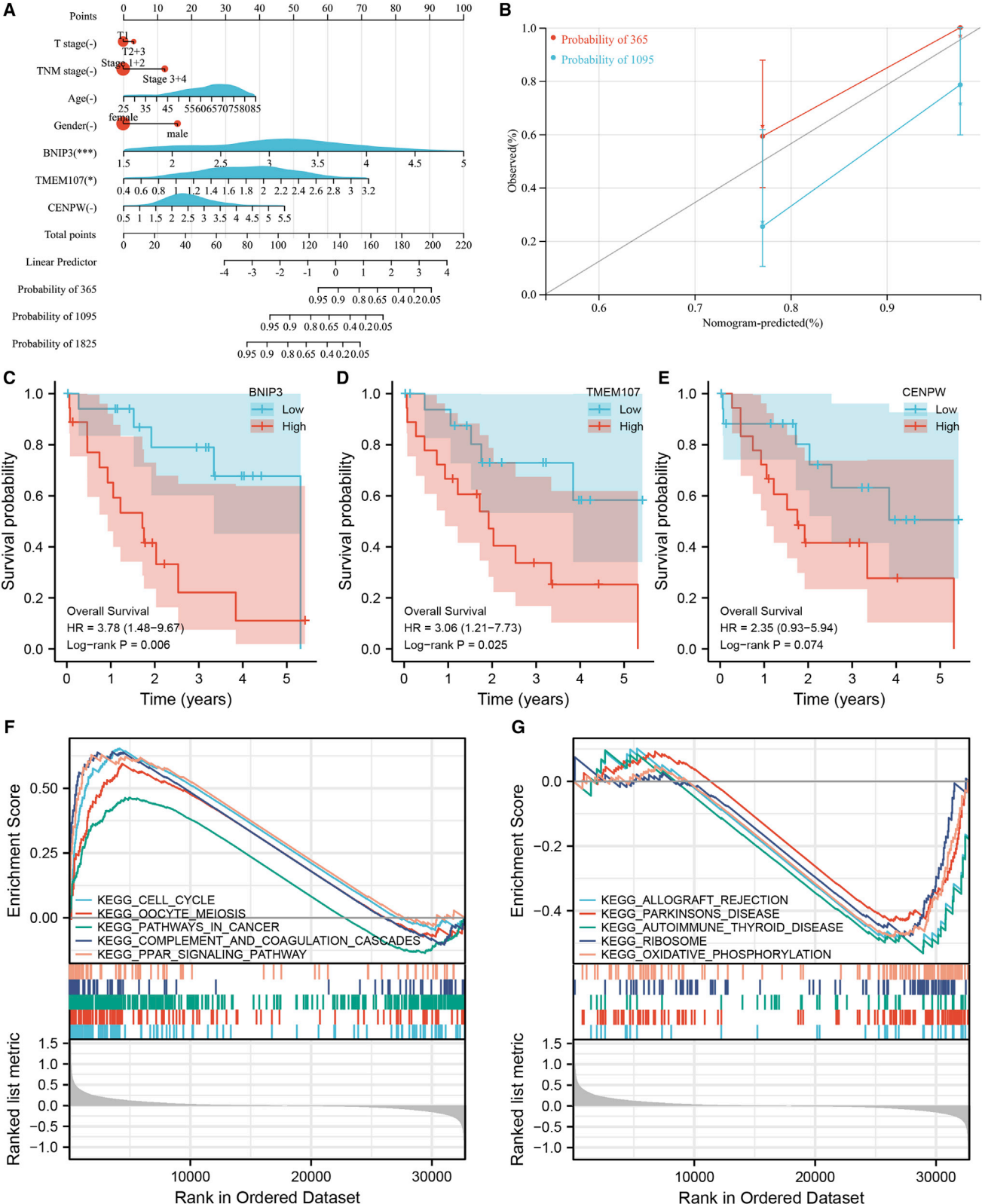
Based on the median value of the F-M signature, the TCGA-CHOL data were divided into high- and low-score groups for KEGG pathway-based gene set enrichment analysis (GSEA) to obtain pathways that may be involved in the regulation of the three genes in the F-M signature. The most significantly upregulated pathways were the cell cycle, oocyte meiosis, pathway in cancer, complement and coagulation cascades, and the peroxisome proliferator-activated receptor signaling pathway (Figure 7F); the most significantly downregulated pathways were allograft rejection, Parkinson's disease, autoimmune thyroid disease, ribosome, and oxidative phosphorylation (Figure 7G).

DISCUSSION

Numerous studies have confirmed the critical role of ferroptosis in killing cancer cells and inhibiting tumor growth.^{20–22} With the in-depth study of tumor immunotherapy, there has been increasing

mechanism for extrahepatic CHOL.²⁵ There are also several articles on prognostic gene signatures of ferroptosis in CHOL, but these articles do not delve into the possible mechanisms of ferroptosis in CHOL.^{26–28}

At tumor sites, monocytes/macrophages constitute the major population of infiltrating leukocytes. Depending on the tumor type, monocytes/macrophages may play a dual role as good or bad indicators of cancer recovery.²⁹ In this study, we used CIBERSORT in the analysis of immune cell infiltration and found that high infiltration of monocytes was associated with a better prognosis (log rank $p < 0.01$). To explore the role of monocytes in malignant cells, we further analyzed the scRNA-seq dataset (GSE138709) and defined 22 cell subsets, including cholangiocytes (clusters 0, 2, and 5; markers STMN1, KRT19, and CLDN4) and monocytes (cluster 3; markers S100A9, S100A8, and LYZ). Intercellular communication analysis showed



(legend on next page)

that the communication relationship between monocytes and cholangiocytes was enriched, and the relationship pair TNFSF13B-TFRC was found. TNFSF13B is a cytokine of the tumor necrosis factor ligand family and one of the recognized markers of monocytes.^{30,31} TFRC is a recognized ferroptosis driver and marker, which acts as a channel of Fe³⁺ in the outer membrane to regulate the occurrence of ferroptosis.^{32–35} We continued to subdivide the cell subsets and identify benign and malignant cholangiocytes and finally found that malignant epithelial cells were significantly enriched in ferroptosis signaling pathways compared with benign epithelial cells, and TFRC was significantly overexpressed in the C4 subset. More interestingly, we also found that the signaling pathway of mineral absorption was significantly enriched, and the enriched genes (FTH1, FTL) in the pathway were closely related to Fe³⁺ transport. Therefore, we speculate that monocyte-derived TNFSF13B promotes the transport of exogenous Fe³⁺ by binding to the TFRC receptor on the surface of C4, thereby inducing the occurrence of the ferroptosis pathway. The results in the single-cell analysis section suggest that monocytes regulate the ferroptosis signaling pathway in CHOL cells through intercellular communication.

On this theoretical basis, using TCGA CHOL data, we screened the monocyte infiltration-related module gene set, obtained the ferroptosis-related gene set through the FerrDb database, and finally obtained the monocyte and ferroptosis gene set. Univariate and multivariate Cox regression analyses were used to construct a prognostic signature of three genes (BNIP3, TMEM107, and CENPW). Subsequently, the reliability of the signature was evaluated in predicting the prognosis of CHOL by using ROC and DCA curves. On this basis, we also constructed a nomogram risk assessment map, which combined the risk score with clinical characteristics to facilitate clinical application.

In recent years, increasing evidence has suggested that BNIP3, TMEM107, and CENPW may be potential targets for CHOL. Using TCGA data and 241 clinical samples, Yuma Wada et al. found and verified that CENPW can be used as one of the gene markers associated with recurrence in patients with intrahepatic CHOL.³⁶ In liver cancer, knockdown of CENPW inhibited cell proliferation, migration, and invasion and induced G0/G1 phase arrest and apoptosis in liver cancer cells.³⁷ Overexpression of CENPW is associated with poor prognosis and may be a potential predictive biomarker for hepatocellular carcinoma.³⁸ BNIP3 is a proapoptotic gene that has been reported to significantly alleviate FTO-dependent tumor growth retardation and metastasis.³⁹ A recent study found that BNIP3 is also one of the marker genes in the occurrence of ferroptosis,⁴⁰ and the lack of BNIP3 can lead to a significant increase in the level of iron in melanoma cells.⁴¹ TMEM107 is a key regulator of cilia composition and Hedgehog signaling and inhibits epithelial-mesenchymal transition and invasion by negatively regulating Hedgehog signaling

in cancer.⁴² BNIP3 and CENPW have also been reported as prognostic predictors in various cancers.^{43–45} These studies confirm the rationality and importance of the prognostic signature in this study.

In conclusion, we started with the impact of immune cell infiltration on prognosis in CHOL, and from the data analysis of single-cell sequencing, we found the possible regulatory mechanism of monocytes on malignant intracellular ferroptosis. Our work not only expands the knowledge of cancer cell ferroptosis in the tumor micro-environment but also provides an F-M signature in the combined TCGA-CHOL and FerrDb databases. The combined analysis of single-cell data and TCGA-CHOL data has identified the three-gene signature with important prognostic implications and implications for immunotherapy in CHOL.

MATERIALS AND METHODS

Data download

CHOL scRNA-seq data GSE138709, including five tumor tissues, three adjacent tissues, 33,694 genes, and 40,919 cells, were downloaded from GEO databases. TCGA-CHOL contains bulk RNA-seq data and corresponding clinical information from 36 CHOL and four paracancerous tissues. GSE107943 contains mRNA sequencing data and clinical information from 30 CHOL samples and 27 paracancerous tissues. The TCGA-CHOL data were downloaded from the UCSC Xena link (<http://www.genome.ucsc.edu/index.html>). Data from the GSE107943 dataset were downloaded from the NCBI GEO link (<https://www.ncbi.nlm.nih.gov/geo/>).

CIBERSORT estimation and Kaplan-Meier survival analysis

The CIBERSORT algorithm was utilized to assess the 22 kinds of immune cell types in pancreatic ductal adenocarcinoma. We used K-M survival analysis to appraise diversities in the CHOL (overall survival) between the high abundance and low abundance of all immune cells. The R packages survMiner and survival were tools to enable this process.

scRNA-seq data processing

The Seurat package SCTransform () function was used to preprocess the single-cell transcriptome datasets. All functions were run with default parameters, unless specified otherwise. We excluded cells with fewer than 200 or more than 6,000 detected genes (where each gene had to have at least one unique molecular identifier aligned in at least three cells). And cells with more than 10 percent expression of mitochondria genes were excluded to remove low activity cells. The most changed 3,000 genes were chosen by SelectIntegrationFeatures () and the FindCluster () package used for all cell cluster analysis with the resolution set to 0.5.

Cell-cell communication analysis was conducted with the scRNA-seq data by using the CellPhoneDB software (version v2.0.0) (www.cellphonedb.org/).

Figure 7. The nomogram of the signature and single-gene K-M survival curve

(A) and (B) are the nomogram and calibration curve of the signature, respectively. (C–E) K-M survival curves according to BNIP3, TMEM107, and CENPW. (F, G) GSEA functional enrichment analysis of high- and low-risk groups: the most highly regulated pathways (F) and the lowest regulated pathways (G).

cellphonedb.org). Only receptors and ligands expressed in >10% of cells of any type from cancer or paracancer group were further evaluated, while a cell-cell communication was considered nonexistent if the ligand or the receptor was unmeasurable. Averaged expression of each ligand-receptor pair was analyzed between various cell types, and only those with p value < 0.01 were used for the prediction of cell-cell communication between any two cell types.

The CNV evaluation based on scRNA-seq data was conducted by *infercnv* R package. We chose hidden Markov model to predict the CNV states. Gene location data were from *AnnoProbe* R package. Subclones of specific subtypes were divided by hierarchy clustering based on CNV. Subclone was clustered by *SC3* R package.

Functional enrichment analysis in Metascape

Gene Ontology terms and KEGG pathway enrichment analyses play a vital role in identifying characteristic biological attributes for high-throughput transcriptome data. We used Metascape (<http://metascape.org>), a gene annotation and analysis resource,⁴⁶ to perform a functional enrichment analysis, which included cellular component, molecular function, and biological process, and a KEGG pathway analysis of the hub genes.

Weighted gene co-expression analysis

Co-expression networks were created utilizing the "WGCNA" package in R software. The CHOL samples in the TCGA databases were clustered to determine the existence of remarkable outliers. Following this, the co-expression network was developed utilizing the automatic network construction function, and the soft threshold was computed using the *pickSoftThreshold* function. The co-expression similarity was derived according to the soft threshold, and the adjacency was calculated thereafter. Next, the modules were ascertained using hierarchical clustering as well as dynamic tree-cut functions. Finally, gene significance as well as module membership were determined to correlate modules with monocytes cell content.

FerrDb database

FerrDb (<http://www.zhounan.org/ferrdb/>) is the first specialized ferroptosis regulatory gene and disease database that summarizes the possible ferroptosis marker genes that can upregulate or downregulate ferroptosis.⁴⁷ We extracted and merged all types of ferroptosis genes in this database and ultimately obtained 588 ferroptosis genes.

Risk signature construction

First, monocytes and ferroptosis genes related to CHOL prognosis were screened by univariate Cox analysis; $p < 0.05$ represented the prognosis-related genes. Subsequently, multivariate Cox analysis was performed on monocytes and ferroptosis genes associated with prognosis to construct a risk signature. The model formula was as described previously, and the coefficients in the formula were obtained by multivariate Cox regression analysis. The protein-protein interaction network was made with Genemania (<http://genemania.org/>).⁴⁸

The ROC curve analysis and DCA were used to evaluate the accuracy of the signature in the training dataset and testing dataset.

Nomogram

In this study, we used the R software package "rms" to integrate survival time, survival status, T stage, TNM stage, age, gender, and the expression levels of BNIP3, TMEM107, and CENPW, and we used the Cox analysis to build a nomogram. We assessed the prognostic significance of these features in the TCGA samples and assessed the power of the nomogram by means of calibration curves and ROC curves.

Gene set enrichment analysis

The GSEA method was used to explore the potential KEGG pathway implicated in the high-risk group and low-risk group. The reference gene set was retrieved from *c2.cp.kegg.v7.1.symbols* files, and the significant pathways were screened based on the criterion: $p < 0.05$ and FDR < 0.25.

Statistical analysis

The statistical analysis was performed in R software (version 4.0.2). K-M survival curve analysis with log rank test was applied to analyze overall survival. Univariate and multivariate Cox regression analyses were used to evaluate prognostic significance. ROC curve analysis and its AUC value was used to evaluate the reliability and sensitivity of the prognostic signature. $p < 0.05$ was regarded as statistically significant.

Data and code availability

The original contributions presented in the study are included in the article, and further inquiries can be directed to the corresponding author.

ACKNOWLEDGMENTS

This study was supported by the National Natural Science Foundation of China (No. 82100675); Heilongjiang Province Education Science "14th Five-Year Plan" 2022 Key Issues (No. GJB1422769); Harbin Engineering University "Biomedical Materials" Postdoctoral Research Workstation (No. 2018CBME/Y03); Harbin Engineering University (No. 2021HX015). The authors also acknowledge the researchers and staff of TCGA and GEO public databases for providing data on cholangiocarcinoma.

AUTHOR CONTRIBUTIONS

W.Y., X.L., D.X., and X.M. contributed to conception and design of the study. W.Y. and X.L. wrote the manuscript. Y.H., M.T., and S.L. performed the statistical analysis. Q.W., Y.Z., and Z.L. prepared the figures. C.H., D.X., and X.M. reviewed the article. C.H. and X.M. performed funding acquisition. All authors have read and approved the final manuscript.

DECLARATION OF INTERESTS

The authors declare no competing interests.

REFERENCES

- Banales, J.M., Cardinale, V., Carpino, G., Marzioni, M., Andersen, J.B., Invernizzi, P., Lind, G.E., Folseraas, T., Forbes, S.J., Fouassier, L., et al. (2016). Expert consensus document: cholangiocarcinoma: current knowledge and future perspectives consensus statement from the European Network for the Study of Cholangiocarcinoma (ENS-CCA). *Nat. Rev. Gastroenterol. Hepatol.* *13*, 261–280.
- Rizvi, S., and Gores, G.J. (2013). Pathogenesis, diagnosis, and management of cholangiocarcinoma. *Gastroenterology* *145*, 1215–1229.
- Chua, D., Low, A., Koh, Y., Goh, B., Cheow, P.C., Kam, J.H., Teo, J.Y., Tan, E.K., Chung, A., Ooi, L.L., et al. (2018). A retrospective review of correlative radiological assessment and surgical exploration for hilar cholangiocarcinoma. *Ann. Hepatobiliary. Pancreat. Surg.* *22*, 216–222.
- Wang, Z., and Du, Y. (2021). Identification of a novel mutation gene signature HAMP for cholangiocarcinoma through comprehensive TCGA and GEO data mining. *Int. Immunopharmacol.* *99*, 108039.
- Capelletti, M.M., Manceau, H., Puy, H., and Peoc'h, K. (2020). Ferroptosis in liver diseases: an overview. *Int. J. Mol. Sci.* *21*, E4908.
- Liao, P., Wang, W., Wang, W., Kryczek, I., Li, X., Bian, Y., Sell, A., Wei, S., Grove, S., Johnson, J.K., et al. (2022). CD8(+) T cells and fatty acids orchestrate tumor ferroptosis and immunity via ACSL4. *Cancer Cell* *40*, 365–378.e6.
- Jiang, M., Qiao, M., Zhao, C., Deng, J., Li, X., and Zhou, C. (2020). Targeting ferroptosis for cancer therapy: exploring novel strategies from its mechanisms and role in cancers. *Transl. Lung Cancer Res.* *9*, 1569–1584.
- Wohlhieter, C.A., Richards, A.L., Uddin, F., Hulton, C.H., Quintanal-Villalonga, À., Martin, A., de Stanchina, E., Bhanot, U., Asher, M., Shah, N.S., et al. (2020). Concurrent mutations in STK11 and KEAP1 promote ferroptosis protection and SCD1 dependence in lung cancer. *Cell Rep.* *33*, 108444.
- Wang, Y., Zheng, L., Shang, W., Yang, Z., Li, T., Liu, F., Shao, W., Lv, L., Chai, L., Qu, L., et al. (2022). Wnt/beta-catenin signaling confers ferroptosis resistance by targeting GPX4 in gastric cancer. *Cell Death Differ.* *49*, 4953.
- Rademaker, G., Boumahd, Y., Peiffer, R., Anania, S., Wissocq, T., Liégeois, M., Luis, G., Sounni, N.E., Agirman, F., Maloujahmoum, N., et al. (2022). Myoferlin targeting triggers mitophagy and primes ferroptosis in pancreatic cancer cells. *Redox Biol.* *53*, 102324.
- Liu, Y., Liu, X., Wang, H., Ding, P., and Wang, C. (2022). Agrimonolide inhibits cancer progression and induces ferroptosis and apoptosis by targeting SCD1 in ovarian cancer cells. *Phytomedicine* *101*, 154102.
- Li, S., He, Y., Chen, K., Sun, J., Zhang, L., He, Y., Yu, H., and Li, Q. (2021). RSL3 drives ferroptosis through NF- κ B pathway activation and GPX4 depletion in glioblastoma. *Oxid. Med. Cell. Longev.* *2021*, 2915019.
- Li, J., Smalley, I., Chen, Z., Wu, J.Y., Phadke, M.S., Teer, J.K., Nguyen, T., Karreth, F.A., Koomen, J.M., Sarnaik, A.A., et al. (2022). Single-cell characterization of the cellular landscape of acral melanoma identifies novel targets for immunotherapy. *Clin. Cancer Res.* *28*, 2131–2146.
- Lei, Y., Tang, R., Xu, J., Wang, W., Zhang, B., Liu, J., Yu, X., and Shi, S. (2021). Applications of single-cell sequencing in cancer research: progress and perspectives. *J. Hematol. Oncol.* *14*, 91.
- Hong, M., Tao, S., Zhang, L., Diao, L.T., Huang, X., Huang, S., Xie, S.J., Xiao, Z.D., and Zhang, H. (2020). RNA sequencing: new technologies and applications in cancer research. *J. Hematol. Oncol.* *13*, 166.
- Rantalainen, M. (2018). Application of single-cell sequencing in human cancer. *Brief. Funct. Genomics* *17*, 273–282.
- Zhang, M., Yang, H., Wan, L., Wang, Z., Wang, H., Ge, C., Liu, Y., Hao, Y., Zhang, D., Shi, G., et al. (2020). Single-cell transcriptomic architecture and intercellular crosstalk of human intrahepatic cholangiocarcinoma. *J. Hepatol.* *73*, 1118–1130.
- Chen, Z., Wang, Y., Li, D., Le, Y., Han, Y., Jia, L., Yan, C., Tian, Z., Song, W., Li, F., et al. (2022). Single-cell RNA sequencing revealed a 3-gene panel predicted the diagnosis and prognosis of thyroid papillary carcinoma and associated with tumor immune microenvironment. *Front. Oncol.* *12*, 862313.
- Wu, J., Minikes, A.M., Gao, M., Bian, H., Li, Y., Stockwell, B.R., Chen, Z.N., and Jiang, X. (2019). Intercellular interaction dictates cancer cell ferroptosis via NF2-YAP signaling. *Nature* *572*, 402–406.
- Mou, Y., Wang, J., Wu, J., He, D., Zhang, C., Duan, C., and Li, B. (2019). Ferroptosis, a new form of cell death: opportunities and challenges in cancer. *J. Hematol. Oncol.* *12*, 34.
- Stockwell, B.R., Jiang, X., and Gu, W. (2020). Emerging mechanisms and disease relevance of ferroptosis. *Trends Cell Biol.* *30*, 478–490.
- Tang, D., Chen, X., Kang, R., and Kroemer, G. (2021). Ferroptosis: molecular mechanisms and health implications. *Cell Res.* *31*, 107–125.
- Tang, R., Xu, J., Zhang, B., Liu, J., Liang, C., Hua, J., Meng, Q., Yu, X., and Shi, S. (2020). Ferroptosis, necroptosis, and pyroptosis in anticancer immunity. *J. Hematol. Oncol.* *13*, 110.
- Günes Günsel, G., Conlon, T.M., Jeridi, A., Kim, R., Ertüz, Z., Lang, N.J., Ansari, M., Novikova, M., Jiang, D., Strunz, M., et al. (2022). The arginine methyltransferase PRMT7 promotes extravasation of monocytes resulting in tissue injury in COPD. *Nat. Commun.* *13*, 1303.
- Han, J.Y., Ahn, K.S., Baek, W.K., Suh, S.I., Kim, Y.H., Kim, T.S., and Kang, K.J. (2020). Usefulness of bile as a biomarker via ferroptosis and cysteine prenylation in cholangiocarcinoma; role of diagnosis and differentiation from benign biliary disease. *Surg. Oncol.* *34*, 174–181.
- Zhang, Z.J., Huang, Y.P., Li, X.X., Liu, Z.T., Liu, K., Deng, X.F., Xiong, L., Zou, H., and Wen, Y. (2021). A novel ferroptosis-related 4-gene prognostic signature for cholangiocarcinoma and photodynamic therapy. *Front. Oncol.* *11*, 747445.
- Wang, Z., Chen, X., and Jiang, Z. (2022). Immune infiltration and a ferroptosis-related gene signature for predicting the prognosis of patients with cholangiocarcinoma. *Am. J. Transl. Res.* *14*, 1204–1219.
- Wang, Z., Zhang, Y., Chen, Y., Liu, S., Li, C., and Li, X. (2022). Identification of a ferroptosis-related gene signature for predicting the prognosis of cholangiocarcinoma. *Expert Rev. Gastroenterol. Hepatol.* *16*, 181–191.
- Alwani, A., Andreasik, A., Szatanek, R., Siedlar, M., and Baj-Krzyworzeka, M. (2022). The role of miRNA in regulating the fate of monocytes in health and cancer. *Biomolecules* *12*, 100.
- Panwar, B., Schmiedel, B.J., Liang, S., White, B., Rodriguez, E., Kalunian, K., McKnight, A.J., Soloff, R., Seumois, G., Vijayanand, P., and Ay, F. (2021). Multi-cell type gene coexpression network analysis reveals coordinated interferon response and cross-cell type correlations in systemic lupus erythematosus. *Genome Res.* *31*, 659–676.
- Chen, Z., Zhang, T., Mao, K., Shao, X., Xu, Y., Zhu, M., Zhou, H., Wang, Q., Li, Z., Xie, Y., et al. (2021). A single-cell survey of the human glomerulonephritis. *J. Cell. Mol. Med.* *25*, 4684–4695.
- Gao, M., Monian, P., Quadri, N., Ramasamy, R., and Jiang, X. (2015). Glutaminolysis and transferrin regulate ferroptosis. *Mol. Cell* *59*, 298–308.
- Gao, M., Monian, P., Pan, Q., Zhang, W., Xiang, J., and Jiang, X. (2016). Ferroptosis is an autophagic cell death process. *Cell Res.* *26*, 1021–1032.
- Shang, Y., Luo, M., Yao, F., Wang, S., Yuan, Z., and Yang, Y. (2020). Ceruloplasmin suppresses ferroptosis by regulating iron homeostasis in hepatocellular carcinoma cells. *Cell. Signal.* *72*, 109633.
- Song, X., Xie, Y., Kang, R., Hou, W., Sun, X., Epperly, M.W., Greenberger, J.S., and Tang, D. (2016). FANCD2 protects against bone marrow injury from ferroptosis. *Biochem. Biophys. Res. Commun.* *480*, 443–449.
- Wada, Y., Shimada, M., Yamamura, K., Toshima, T., Banwait, J.K., Morine, Y., Ikemoto, T., Saito, Y., Baba, H., Mori, M., and Goel, A. (2021). A transcriptomic signature for risk-stratification and recurrence prediction in intrahepatic cholangiocarcinoma. *Hepatology* *74*, 1371–1383.
- Zhou, Y., Chai, H., Guo, L., Dai, Z., Lai, J., Duan, J., Liu, Y., and Ding, Q. (2021). Knockdown of CENPW inhibits hepatocellular carcinoma progression by inactivating E2F signaling. *Technol. Cancer Res. Treat.* *20*, 15330338211007253.
- Zhou, Z., Zhou, Z., Huang, Z., He, S., and Chen, S. (2020). Histone-fold centromere protein W (CENP-W) is associated with the biological behavior of hepatocellular carcinoma cells. *Bioengineered* *11*, 729–742.
- Niu, Y., Lin, Z., Wan, A., Chen, H., Liang, H., Sun, L., Wang, Y., Li, X., Xiong, X.F., Wei, B., et al. (2019). RNA N6-methyladenosine demethylase FTO promotes breast tumor progression through inhibiting BNIP3. *Mol. Cancer* *18*, 46.

40. Yang, W.S., SriRamaratnam, R., Welsch, M.E., Shimada, K., Skouta, R., Viswanathan, V.S., Cheah, J.H., Clemons, P.A., Shamji, A.F., Clish, C.B., et al. (2014). Regulation of ferroptotic cancer cell death by GPX4. *Cell* *156*, 317–331.
41. Vara-Pérez, M., Rossi, M., Van den Haute, C., Maes, H., Sassano, M.L., Venkataramani, V., Michalke, B., Romano, E., Rillaerts, K., Garg, A.D., et al. (2021). BNIP3 promotes HIF-1 α -driven melanoma growth by curbing intracellular iron homeostasis. *EMBO J.* *40*, e106214.
42. Xu, H., Dun, S., Gao, Y., Ming, J., Hui, L., and Qiu, X. (2021). TMEM107 inhibits EMT and invasion of NSCLC through regulating the Hedgehog pathway. *Thorac. Cancer* *12*, 79–89.
43. Lu, W., Wu, Y., Huang, S., and Zhang, D. (2021). A ferroptosis-related gene signature for predicting the prognosis and drug sensitivity of head and neck squamous cell carcinoma. *Front. Genet.* *12*, 755486.
44. Zhou, Z., Yang, Z., Cui, Y., Lu, S., Huang, Y., Che, X., Yang, L., and Zhang, Y. (2022). Identification and validation of a ferroptosis-related long non-coding RNA (FRLncRNA) signature to predict survival outcomes and the immune microenvironment in patients with clear cell renal cell carcinoma. *Front. Genet.* *13*, 787884.
45. Hou, S., Xu, H., Liu, S., Yang, B., Li, L., Zhao, H., and Jiang, C. (2022). Integrated bioinformatics analysis identifies a new stemness index-related survival model for prognostic prediction in lung adenocarcinoma. *Front. Genet.* *13*, 860268.
46. Zhou, Y., Zhou, B., Pache, L., Chang, M., Khodabakhshi, A.H., Tanaseichuk, O., Benner, C., and Chanda, S.K. (2019). Metascape provides a biologist-oriented resource for the analysis of systems-level datasets. *Nat. Commun.* *10*, 1523.
47. Zhou, N., and Bao, J. (2020). FerrDb: A manually curated resource for regulators and markers of ferroptosis and ferroptosis-disease associations. *Database (Oxford)*.
48. Warde-Farley, D., Donaldson, S.L., Comes, O., Zuberi, K., Badrawi, R., Chao, P., Franz, M., Grouios, C., Kazi, F., Lopes, C.T., et al. (2010). The GeneMANIA prediction server: biological network integration for gene prioritization and predicting gene function. *Nucleic Acids Res.* *38*, W214–W220.